Shahrokh Zeinali-Davarani
Department of Mechanical Engineering,
Boston University,
Boston, MA 02215

Yunjie Wang
Department of Mechanical Engineering,
Boston University,
Boston, MA 02215

Ming-Jay Chow
Department of Mechanical Engineering,
Boston University,
Boston, MA 02215

Raphaël Turcotte
Department of Biomedical Engineering,
Boston University,
Boston, MA 02215;
Advanced Microscopy Program,
Center for Systems Biology
and Wellman Center for Photomedicine,
Massachusetts General Hospital,
Harvard Medical School,
Boston, MA 02114

Yanhang Zhang[1]
Department of Mechanical Engineering,
Boston University,
Boston, MA 02215;
Department of Biomedical Engineering,
Boston University,
Boston, MA 02215
e-mail: yanhang@bu.edu

Contribution of Collagen Fiber Undulation to Regional Biomechanical Properties Along Porcine Thoracic Aorta

As major extracellular matrix components, elastin, and collagen play crucial roles in regulating the mechanical properties of the aortic wall and, thus, the normal cardiovascular function. The mechanical properties of aorta, known to vary with age and multitude of diseases as well as the proximity to the heart, have been attributed to the variations in the content and architecture of wall constituents. This study is focused on the role of layer-specific collagen undulation in the variation of mechanical properties along the porcine descending thoracic aorta. Planar biaxial tensile tests are performed to characterize the hyperelastic anisotropic mechanical behavior of tissues dissected from four locations along the thoracic aorta. Multiphoton microscopy is used to image the associated regional microstructure. Exponential-based and recruitment-based constitutive models are used to account for the observed mechanical behavior while considering the aortic wall as a composite of two layers with independent properties. An elevated stiffness is observed in distal regions compared to proximal regions of thoracic aorta, consistent with sharper and earlier collagen recruitment estimated for medial and adventitial layers in the models. Multiphoton images further support our prediction that higher stiffness in distal regions is associated with less undulation in collagen fibers. Recruitment-based models further reveal that regardless of the location, collagen in the media is recruited from the onset of stretching, whereas adventitial collagen starts to engage with a delay. A parameter sensitivity analysis is performed to discriminate between the models in terms of the confidence in the estimated model parameters.
[DOI: 10.1115/1.4029637]

Keywords: regional variation, recruitment-based constitutive models, collagen undulation, multiphoton microscopy, biaxial tensile test, parameter sensitivity analysis

Introduction

Aortic wall mechanical properties are essential to the normal cardiovascular function by modulating the blood pressure and flow [1,2]. Composition and architecture of structural proteins within aortic wall regulate its large deformation and orthotropic mechanical response [3,4]. Elastin contributes to the flexibility and resilience of the aorta and is considered to be mainly responsible for the passive elastic behavior under low stretch while collagen fibers are still undulated. Collagen progressively engages in load bearing at medium to high stretch and dominates the mechanical response [5,6].

Content and architecture of elastin and collagen and, hence, the mechanics of aorta vary not only with disease and aging (see review by Tsamis et al. [7]) but also with anatomical locations throughout the aortic tree [8–13]. For instance, elastin content [14–17] and the number of lamellar units [18,19] appear to drop markedly from proximal thoracic to distal regions of aorta. Purslow [20] reported an increase in stiffness and ultimate tensile strength in circumferential and longitudinal directions along the thoracic aorta from the first to the sixth intercoastal arteries. Using uniaxial tensile device, Sokolis [15] characterized the wall mechanical properties of multiple segments along the porcine aorta and found that regions proximal to the heart are stiffer at low stretch levels which was attributed to higher elastin content. Whereas distal abdominal aortas were found to be stiffer at medium and high stretch levels due to higher collagen content. Inflation tests of mice aorta showed that the circumferential elastic modulus is the highest in the distal thoracic aorta close to the diaphragm [21]. Haskett et al. [22] performed biaxial tensile experiment on human aortas and found an increasing trend in circumferential and axial tangent modulus from the aortic arch to the abdominal aorta. Through constitutive modeling, Rachev et al. [23] showed that higher collagen mass fraction and lower elastin mass fraction are associated with reduced compliance along the aorta and fulfill the uniform distribution of wall stress across the thickness and along the aorta.

In most of the previous studies, the variations in mechanical properties have been mainly linked to the variations in elastin and collagen contents or their ratio. However, microstructural properties and in particular the collagen undulation and its engagement are speculated to contribute to the alterations in biomechanical properties of aorta [24–26]. On the other hand, in a our recent study a clear sequence for the engagement of collagen fibers was identified between layers of aorta using microscopic imaging of biaxially loaded tissues [27]. There is a need for more studies on the longitudinal as well as through thickness variations in collagen undulation and their association with the mechanical behavior of aorta to provide a better understanding of its structure–function relationship.

In this study, we perform planar biaxial tensile tests to characterize the regional mechanical properties along the porcine descending thoracic aorta. We use bilayer structurally motivated constitutive models to account for the spatial variations in the

[1]Corresponding author.

Manuscript received August 13, 2014; final manuscript received December 24, 2014; published online February 20, 2015. Assoc. Editor: Hai-Chao Han.

collagen undulation as well as the corresponding mechanical properties and support our modeling predictions with multiphoton imaging. The goal of this study is not only to study the contribution of collagen undulation to the mechanical properties along the thoracic aorta but also to reveal the layer-specific dynamics of collagen engagement using bilayer constitutive models.

Materials and Methods

Sample Preparation and Mechanical Testing. Porcine aortas ($n = 3$) from 12 to 24 month-old pigs are obtained from a local slaughter house and cleaned of excess tissues. Four equal pieces are cut along the thoracic section side-by-side, named as: *proximal, midproximal, mid-distal, and distal*. From each piece, a square sample of $\sim 1.5 \times 1.5$ cm is prepared for biaxial tensile testing using a custom designed device [28,29] while another sample of $\sim 2.0 \times 2.0$ cm is reserved for multiphoton microscopic imaging. Samples are preconditioned through eight loading cycles up to 30 N/m. Following the preconditioning cycles, a preload of 2 ± 0.050 N/m is applied in order to flatten the arterial samples and to keep sutures straightened. The preloaded configuration is chosen as the reference configuration for stress and stretch calculations. Eight cycles of one equibiaxial and four nonequibiaxial tensions are applied to each sample according to the following protocols: $f_l{:}f_c = 1{:}2,\ 2{:}3,\ 1{:}1,\ 3{:}2,\ 2{:}1$. Where $f_l{:}f_c$ is the ratio of tensions applied in longitudinal and circumferential directions, respectively.

Constitutive Modeling. Various phenomenological or structurally motivated constitutive formulations have been proposed in vascular mechanics (see reviews by Holzapfel et al. [30], Humphrey [31], and Holzapfel and Ogden [32]). Structural-based constitutive models need to take the layer-specific material properties into consideration [33–38].

Herein, we adopt three structurally motivated constitutive models to fit the biaxial tensile data of each sample. In each model, the aorta is assumed to be formed of two structurally significant layers, i.e., *media* (M) and *adventitia* (A), with independent material parameters such that the total strain energy function is $W = \sum_{i=M,A} W_i$ [37,39,40]. The Cauchy stress is calculated as $\mathbf{T} = -p\mathbf{I} + (\partial W/\partial \mathbf{F})\mathbf{F}^T$, where $\mathbf{F}$ is the deformation gradient and p is a Lagrange multiplier obtained from the incompressibility and plane stress assumptions [1,39]. In the following, we describe the strain energy function for each model:

Model A. An exponential-based model [6,30], assuming each layer $(i = M, A)$ as a composite of amorphous elastin reinforced by two families of symmetric diagonal collagen fibers $(k = 1, 2)$ with the same material parameters $c_1^i > 0$ and $c_2^i > 0$. The strain energy function for the layer i is then given by

$$W_i = \frac{c_e^i}{2}(I_1 - 3) + \sum_{k=1}^{2} \frac{c_1^i}{2c_2^i}\left[\exp\left\{c_2^i\left(\lambda_k^2 - 1\right)^2\right\} - 1\right] \tag{1}$$

where $\lambda_k^2 = \left(\lambda_z \sin\gamma_k^i\right)^2 + \left(\lambda_\theta \cos\gamma_k^i\right)^2$ and γ_k^i is the fiber orientation with respect to the circumference such that $\gamma_1^i = -\gamma_2^i = \gamma^i$. Elastin in each layer i is assumed to behave as a neo-Hookean material with a material constant c_e^i.

Models B and C. Recruitment-based models where collagen fibers within each symmetric diagonal family are assumed to be naturally undulated according to a statistical distribution [41–47]. The strain energy function for the layer i is then given by

$$W_i = \frac{c_e^i}{2}(I_1 - 3) + \sum_{k=1}^{2} \frac{1}{2}\int_0^{E_k} \psi_f^i (E_k - x)\rho_{fk}^i(x)dx \tag{2}$$

where $E_k = 1/2\left(\lambda_k^2 - 1\right)$ is the strain in the direction of fiber family $k = 1, 2$. When straightened, individual collagen fibers are assumed to behave linearly such that $\psi_f^i = 1/2 c_c^i E_k^2$ [44,48–51]. c_c^i is an elastic constant associated with collagen in each layer. In our study, we choose $c_c^A = 200$ Mpa [43,48,50]. Some studies including our own observations suggest that collagen fibrils in the media are significantly thinner than the adventitial collagen [27,52–54]. Also, the media is known to contain a much greater fraction of type III collagen which is considered to be more extensible compared to type I collagen in the adventitia [55]. Therefore, we assume $c_c^M = 1/2 c_c^A$. In Eq. (2), ρ_{fk}^i is the recruitment distribution density function, considered to be a normal distribution (model B) or a Gamma distribution (model C) as the following:

$$\text{Model B}: \rho_{fk}^i(x) = \frac{1}{\sqrt{2\pi} d_k^i}\exp\left(-\frac{\left(x - m_k^i\right)^2}{2\left(d_k^i\right)^2}\right) \tag{3}$$

where $m_k^i > 0$ and $d_k^i > 0$ represent the mean and standard deviation of the normal distribution, defining the shape of the recruitment of collagen fibers within layer i. Note that assuming the symmetric fiber families $m_1^i = m_2^i$ and $d_1^i = d_2^i$.

$$\text{Model C}: \rho_{fk}^i(x) = \frac{x^{\alpha_k^i - 1}}{\beta_k^i \alpha_k^i \Gamma\left(\alpha_k^i\right)}\exp\left(-\frac{x}{\beta_k^i}\right) \tag{4}$$

where $\alpha_k^i > 0$ and $\beta_k^i > 0$ are the shape and scale parameters of the Gamma distribution associated with the fiber family k and the layer i such that $\alpha_1^i = \alpha_2^i$ and $\beta_1^i = \beta_2^i$.

Parameter Estimation. Best fit parameters associated with the constitutive relations are independently estimated for each aortic sample by minimizing the difference between the calculated and the experimentally obtained stresses. All loading protocols are included in the minimization process except for the equibiaxial tension (1:1) case which is used after the parameter estimation to examine the predictive capability of the models with the best fit parameters. The objective function to minimize is [1]

$$S = \sum_{i=1}^{n}\left\{\left(T_{zz}^c - T_{zz}^e\right)_i^2 + \left(T_{\theta\theta}^c - T_{\theta\theta}^e\right)_i^2\right\} \tag{5}$$

where n is the sample size and subscripts z and θ correspond to the longitudinal and circumferential directions. A direct search method, built in MATLAB Optimization toolbox, is employed to minimize the objective function. Given the fact that elastin mainly presents in the medial layer [15,27,30,49], the contribution of elastin in the adventitial layer was assumed to be minimal by constraining the corresponding parameter $\left(c_e^A < 5\text{kPa}\right)$. A root-mean-square (RMS) measure of error is calculated for the goodness-of-fit assessment according to Wagner and Humphrey [56]

$$\text{RMS} = \sqrt{\frac{\sum_1^n \left(T_{zz}^c - T_{zz}^e\right)^2}{n}} + \sqrt{\frac{\sum_1^n \left(T_{\theta\theta}^c - T_{\theta\theta}^e\right)^2}{n}} \tag{6}$$

Model Parameter Sensitivity Analysis. In this study, we analytically derived the partial derivatives of Cauchy stress with respect to the constitutive parameters associated with collagen in each model and calculated the dimensionless sensitivity coefficients [57,58] as

$$S_{zi} = \frac{P_i}{T_{zz}}\frac{\partial T_{zz}}{\partial P_i}, \quad S_{\theta i} = \frac{P_i}{T_{\theta\theta}}\frac{\partial T_{\theta\theta}}{\partial P_i} \tag{7}$$

where $P = \left\{c_1^M, c_2^M, c_1^A, c_2^A\right\}$, $\left\{d^{\mathrm{M}}, m^{\mathrm{M}}, d^{\mathrm{A}}, m^{\mathrm{A}}\right\}$ or $\left\{\alpha^{\mathrm{M}}, \beta^{\mathrm{M}}, \alpha^{\mathrm{A}}, \beta^{\mathrm{A}}\right\}$ for models A, B, or C, respectively.

Multiphoton Microscopy. The three-dimensional microstructure of collagen and elastin fibers can be visualized using

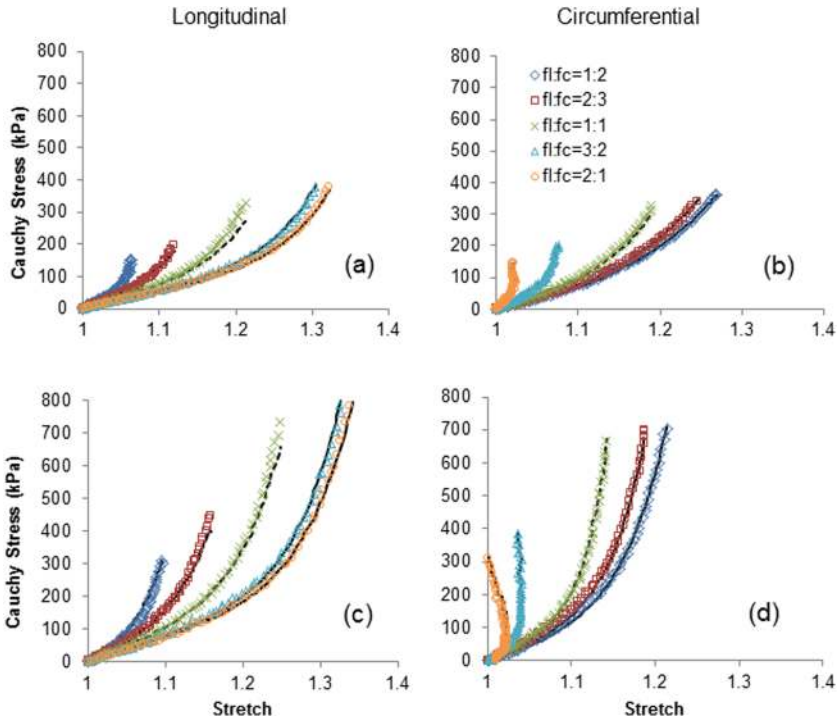

Fig. 1 Representative stress–stretch responses for proximal ((*a*) and (*b*)) and distal ((*c*) and (*d*)) regions of thoracic aorta in the longitudinal and circumferential directions using biaxial loading protocols: f_l:f_c = 1:2, 2:3, 1:1, 3:2, 2:1 (f_l:f_c is the ratio of tensions applied in the longitudinal and circumferential directions). The curves estimated using model B are shown as solid lines while the model response predicted for the equibiaxial tension protocol (f_l:f_c = 1:1) are shown as dashed lines.

multiphoton scanning microscopy. Collagen has a noncentrosymmetric molecular structure which enables label-free imaging with second-harmonic generation (SHG). Label-free imaging is also possible in elastin FAS they have endogenous fluorescence which can be generated by a two-photon excitation process (2PEF) [59]. Three-dimensional imaging is possible due to the nonlinearity of multiphoton processes providing intrinsic optical sectioning and hence depth-resolved measurements. In this study, SHG from collagen (417/80 nm) and 2PEF from elastin (525/45 nm) are generated with a mode-locked Ti:sapphire laser (Maitai-HP, Spectra-Physics) at 800 nm with an average power of 50 MW at the sample. A video-rate scanning microscope is used for image acquisition [60]. A quarter-wave plate positioned before the objective (60X, NA1.0W, LUMPlanN, Olympus) generates the quasi-circular polarization (1.8 dB) required to alleviate the excitation polarization dependence of the SHG signal. Axial-stacks of 100 μm are recorded at nine locations on the adventitia in both distal and proximal regions of arteries ($n = 3$) and maximum intensity projection images were generated.

Waviness Quantification. Given the distance between the end points of a fiber (L) and the fiber length (l), the straightness of fibers (L/l) is quantified for a subset of images of adventitial collagen from proximal and distal regions using NeuronJ [61–66]. A completely straight fiber is represented by $L/l = 1$. Statistical analysis was performed by JMP Pro (version 10.0.2, SAS Institute Inc.) using two-tail two-sample t-test assuming unequal variances with $p < 0.05$ indicating a significant difference.

Results

Representative biaxial stress–stretch data obtained for the proximal and distal regions (of Artery 2) along with the estimated curves using model B are shown in Fig. 1. A stiffer response in both directions is evident in the distal region compared to the proximal region, particularly at higher stretches (Fig. 1). Fitting curves using the other two models are not shown as there is a negligible difference in the goodness-of-fit using all models (RMS error shown in Tables 1–3). In both circumferential and longitudinal directions a precise fit is obtained for nonequibiaxial tension protocols while the predicted model response under the equibiaxial tension (1:1) case also match the data reasonably well ($R^2 > 0.9$). The same behavior has been observed for the four remaining aortas (not shown).

Figure 2 shows the longitudinal and circumferential tangent modulus calculated for the equibiaxial tension stress–strain curves at multiple stretches, averaged between three aortas. Distal samples appear to be stiffer than proximal samples in both longitudinal and circumferential directions and the difference in stiffness dramatically increases with higher stretch. Best fit materials parameters estimated for all samples using models A, B, and C are given in Tables 1–3.

Collagen parameters of model A (c_2^M and c_2^A in Table 1) are shown to increase on average from proximal to distal regions and, for model B (Table 2), the mean values (m^A) and the standard deviations (d^A) of the Normal recruitment distribution appear to be reducing on average from proximal to distal regions. Figure 3 depicts the representative recruitment distribution densities estimated for the proximal and distal regions (of Artery 2) using models B and C. Both medial and adventitial collagen fibers in the distal region seem to engage in load bearing earlier and more abruptly compared to the proximal region. The regional difference in the recruitment is more pronounced collagen fibers in the media.

Moreover, it appears that the medial collagen is recruited gradually from the beginning of loading while the adventitial collagen starts to engage with a delay that is fairly consistent between the two models.

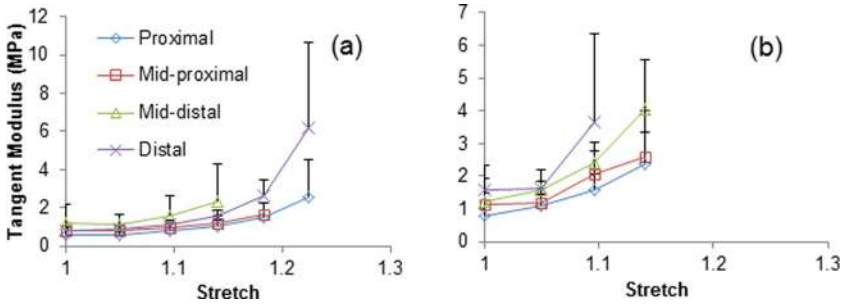

Fig. 2 Average longitudinal (*a*) and circumferential (*b*) tangent modulus at multiple locations (proximal, midproximal, mid-distal, and distal) along the descending thoracic aorta

The convexity of strain energy functions is briefly demonstrated for model B in the Appendix. Meanwhile, Fig. 4 illustrates the 3D contour plots of the strain energy stored in media and adventitia using the estimated parameters of model B for Artery 2. Higher levels of the strain energy stored in the distal region is mostly due to the larger contribution of collagen.

In Fig. 5, the sensitivity coefficients are plotted against the corresponding stretches using the optimal (nominal) sets of model parameters for the proximal region of Artery 2 (Tables 1–3). For model A, sensitivities with respect to c_2^M, c_2^A are less significant compared to c_1^M, c_1^A at low stretch while sensitivity coefficients increase rapidly with stretch. Relatively larger sensitivities are noticeable for parameters of models B and C compared to model A, meaning that models B and C are more sensitive to the variations in their parameters than model A. However, there appears to be a large degree of linear dependency between sensitivity coefficients of model B (with respect to d^i, m^i. in Figs. 5(*c*) and 5(*d*)).

Representative SHG images of medial and adventitial collagen fibers along with 2PEF images of medial elastin from proximal and distal regions are shown in Fig. 6. A highly corrugated collagen structure is noticeable in the proximal adventitia whereas a relatively less undulated structure can be seen in the distal region. We did not notice a significant structural difference in medial collagen and elastin between proximal and distal regions.

Figure 7 compares the straightness of fibers quantified for adventitial collagen in proximal and distal regions. We found that straightness of distal collagen fibers (0.97 ± 0.02) is significantly larger than the straightness of proximal collagen fibers (0.77 ± 0.09).

Discussion

Understanding the regional properties of aortic wall may shed light on pathophysiology of vascular diseases prevalent to specific regions of aorta. To this end, constitutive models that are motivated by the microstructure provide a powerful tool to account for the observed differences in biomechanical properties with the help of advanced microscopic techniques. In this study we performed biaxial tensile tests on aortic samples taken from four different locations along the descending thoracic aorta and employed bilayer structurally motivated constitutive models to account for

Table 1 Parameters of model A estimated for aortic samples at four locations (proximal, midproximal, mid-distal, and distal) along three thoracic aortas

	c_e^M(kPa)	c_e^A(kPa)	c_1^M	c_2^M	c_1^A	c_2^A	γ^M	γ^A	RMS
Proximal									
Artery1	45.48	0.28	154.91	2.39	34.11	1.01	34.68	80.00	52.25
Artery2	83.95	0.17	38.94	5.26	103.10	3.62	57.36	31.49	35.03
Artery3	6.78	2.53	65.34	1.30	246.59	3.01	80.00	34.06	24.38
Artery4	0.00	0.10	56.13	0.77	238.90	1.54	80.00	30.74	28.22
Artery5	12.03	0.15	96.73	0.00	344.94	1.29	80.00	31.44	36.62
Mean	29.65	0.65	82.41	1.94	193.53	2.09	66.41	41.55	
Midproximal									
Artery1	79.32	0.43	126.71	2.61	32.19	2.13	34.64	67.69	47.03
Artery2	45.99	4.25	92.16	3.37	168.66	3.19	53.82	28.46	39.06
Artery3	8.56	0.12	53.79	0.49	269.17	3.11	80.00	33.79	41.31
Artery4	0.00	0.10	70.51	0.53	246.34	0.81	80.00	34.95	33.15
Artery5	0.00	0.10	433.21	1.60	136.71	0.26	34.57	80.00	31.37
Mean	26.77	1.00	155.27	1.72	170.61	1.90	56.61	48.98	
Mid-distal									
Artery1	126.71	5.00	220.42	4.61	74.79	3.30	30.73	66.82	91.61
Artery2	78.65	4.22	138.72	6.72	88.21	3.69	29.30	53.35	54.76
Artery3	0.00	0.10	311.14	5.26	249.69	4.78	30.54	61.86	63.92
Artery4	71.45	5.00	75.67	0.89	123.32	8.08	10.00	47.34	118.17
Artery5	185.75	0.65	75.32	0.27	70.26	10.78	10.00	43.85	86.44
Mean	92.51	2.99	164.26	3.55	121.25	6.12	22.12	54.64	
Distal									
Artery1	63.26	0.19	81.29	8.31	128.22	5.87	14.31	52.92	85.80
Artery2	104.27	1.39	178.76	9.23	57.17	7.02	32.85	55.49	64.51
Artery3	0.00	0.10	458.96	6.79	89.48	1.46	34.81	80.00	72.89
Artery4	102.31	2.53	44.66	11.15	53.96	1.00	43.48	10.00	206.32
Artery5	159.25	4.46	56.64	10.09	73.45	3.74	45.99	10.00	324.79
Mean	85.82	1.73	164.06	9.11	80.45	3.82	34.29	41.68	

Table 2 Parameters of model B estimated for aortic samples at four locations (proximal, midproximal, mid-distal, and distal) along three thoracic aortas

	c_e^M(kPa)	c_e^A(kPa)	d^M	m^M	d^A	m^A	γ^M	γ^A	RMS
Proximal									
Artery1	104.99	5.00	0.43	1.07	0.50	1.74	34.13	73.87	48.22
Artery2	125.26	0.21	0.53	1.26	0.17	0.62	31.43	55.89	29.81
Artery3	117.89	0.92	0.48	1.09	0.29	0.94	30.40	61.28	21.82
Artery4	90.99	4.71	4.95	0.00	0.28	1.03	29.02	66.14	30.53
Artery5	158.34	0.17	4.42	0.00	4.69	8.87	26.95	56.80	41.25
Mean	119.49	2.20	2.16	0.69	1.18	2.64	30.39	62.80	
Midproximal									
Artery1	132.20	5.00	0.33	0.90	0.28	1.06	34.51	66.38	48.34
Artery2	122.88	0.18	4.16	0.00	0.19	0.66	29.28	51.99	32.24
Artery3	114.81	0.12	3.96	1.11	0.32	1.05	29.20	53.79	42.19
Artery4	113.76	0.10	1.75	2.90	1.19	3.47	35.33	80.00	35.51
Artery5	184.93	5.00	3.19	0.00	1.89	4.26	33.36	66.14	32.04
Mean	133.72	2.08	2.68	0.98	0.77	2.10	32.34	63.66	
Mid-distal									
Artery1	229.10	0.16	0.24	0.61	0.20	0.71	30.46	65.46	89.76
Artery2	141.79	5.00	0.26	0.64	0.19	0.64	28.56	50.27	46.21
Artery3	183.88	5.00	0.20	0.50	0.19	0.57	31.12	60.47	57.17
Artery4	114.21	4.99	6.65	0.00	0.22	0.68	26.43	49.35	81.89
Artery5	209.15	2.30	5.29	0.00	0.13	0.48	29.65	47.18	61.03
Mean	175.63	3.49	2.53	0.35	0.19	0.62	29.24	54.55	
Distal									
Artery1	137.28	0.70	0.17	0.50	0.15	0.51	17.12	52.97	90.90
Artery2	175.12	0.12	0.14	0.39	0.12	0.46	32.14	53.01	54.95
Artery3	186.97	0.55	0.20	0.48	0.17	0.54	28.26	51.36	72.25
Artery4	115.99	1.16	8.98	2.79	0.14	0.51	23.91	45.18	119.72
Artery5	181.53	5.00	2.72	3.64	0.12	0.44	14.16	46.38	250.88
Mean	159.38	1.51	2.44	1.56	0.14	0.49	23.12	49.78	

the layer-specific variations in structural and mechanical properties along the aorta.

Variations Along the Length of Aorta. Our results clearly indicated an elevated stiffness (larger contribution of collagen) in the distal thoracic aorta relative to the proximal thoracic aorta (Fig. 1) which is in line with the general perception based on numerous studies. That is, the aortic stiffness increases along the aortic tree from proximal to distal regions [15,22,67]. The reason for this variation is not fully understood although the variation in elastin and collagen content is suspected to be a contributing factor. The current study suggests that the rapid stiffening response

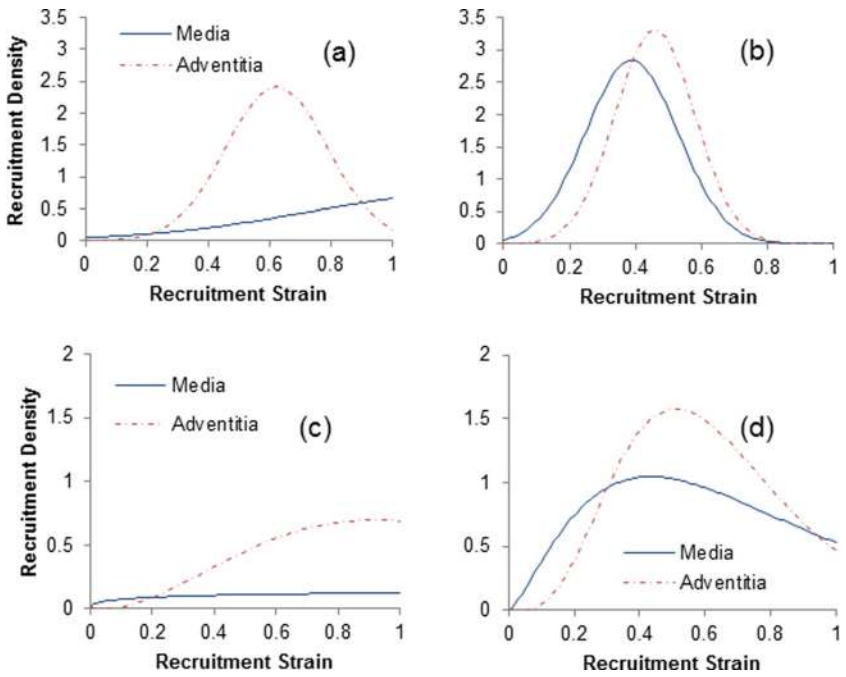

Fig. 3 Recruitment distribution densities estimated for medial and adventitial collagen fibers in the proximal ((*a*) and (*c*)) and distal ((*b*) and (*d*)) thoracic aorta using models B (top panels) and C (bottom panels)

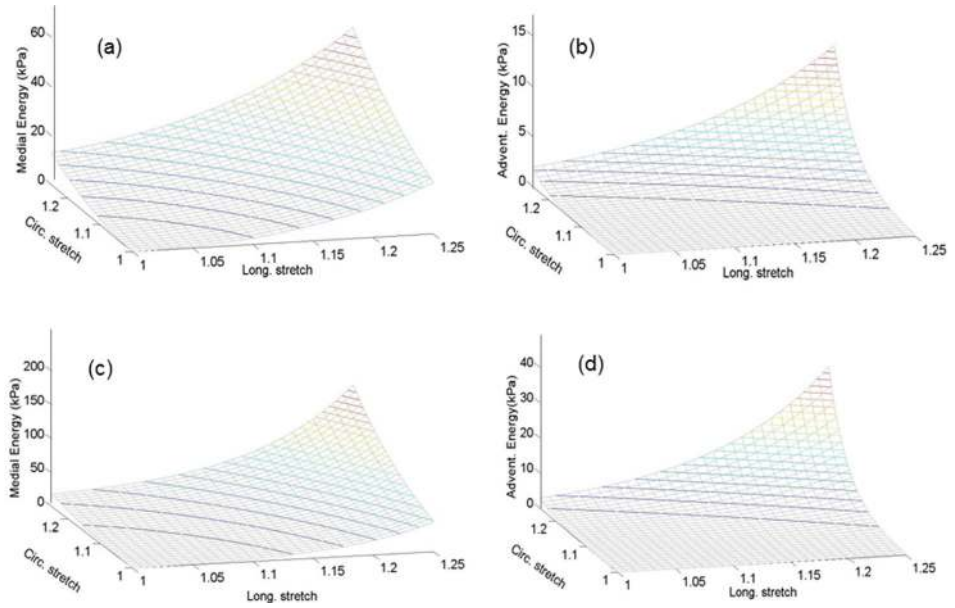

Fig. 4 Three-dimensional contour plots of strain energy stored in media and adventitia given the estimated parameters of model B for proximal ((*a*) and (*b*)) and distal ((*c*) and (*d*)) regions of Artery 2

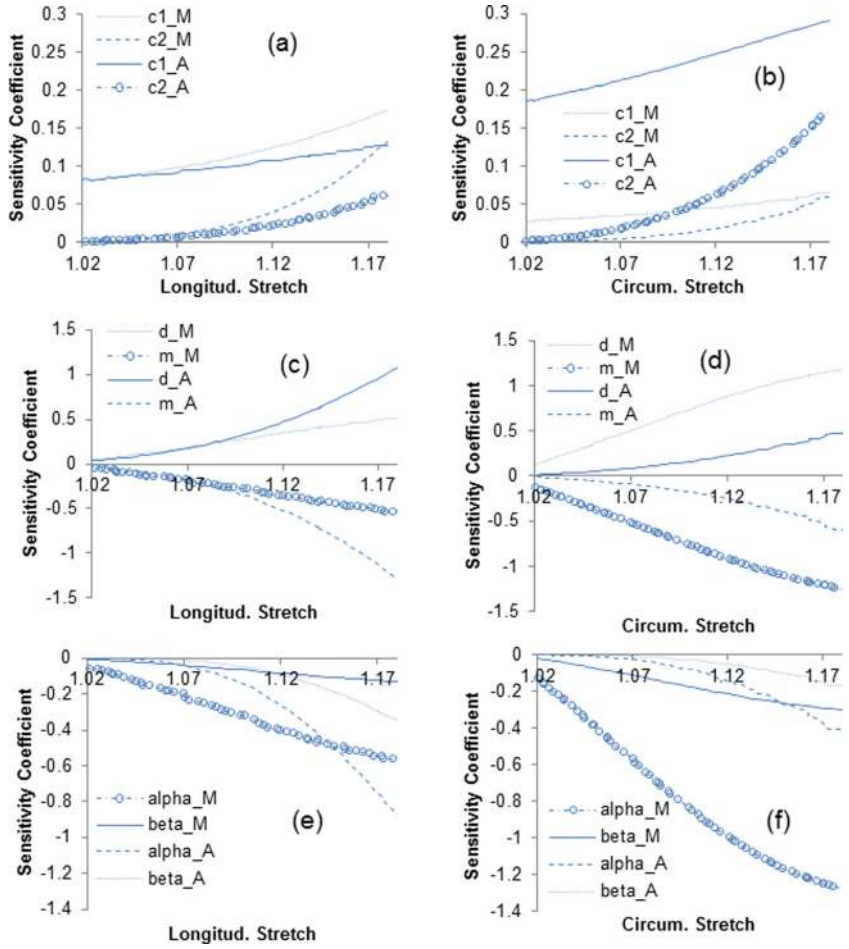

Fig. 5 Sensitivity coefficients of longitudinal and circumferential stress with respect to the constitutive parameters associated with collagen for model A ((*a*) and (*b*)), model B ((*c*) and (*d*)), and model C ((*e*) and (*f*))

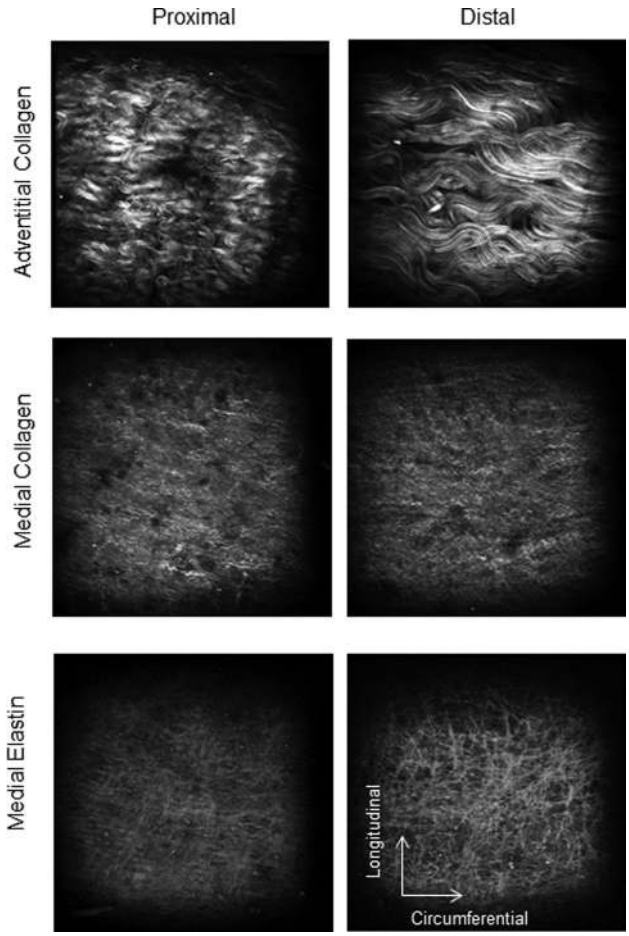

Fig. 6 Representative SHG images of collagen in media and adventitia and 2PEF images of elastin in media of proximal (left column) and distal (right column) regions of thoracic aortas. Adventitial collagen fibers are highly undulated in the proximal region compared to the distal region while there is no obvious difference in medial elastin and collagen waviness between proximal and distal region (images 360 × 360 μm).

of distal samples may also be explained with less undulation in collagen fibers in both media and adventitia (Figs. 3(*b*) and 3(*d*)). Less undulation of fibers (in a load-free configuration) leads to a rapid recruitment as the fibers become straight upon loading. The association between higher undulation of collagen fibers and higher compliance of proximal region of the thoracic aorta

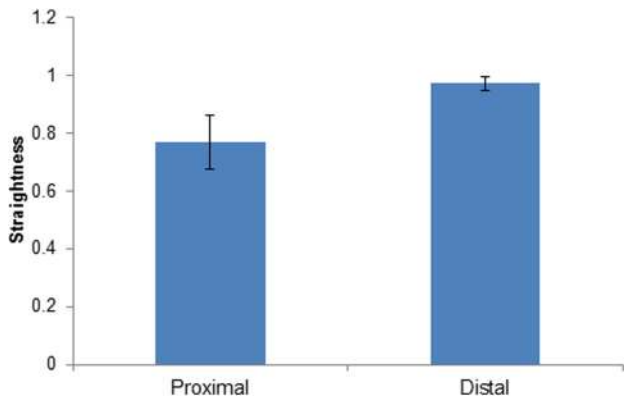

Fig. 7 Mean and standard deviation of adventitial collagen fibers straightness measured at proximal and distal regions ($p < 0.05$)

corroborates the stronger pulse-dampening function of proximal aorta in dampening the pulsatile output of the left ventricle.

The underlying structural differences in adventitial collagen fibers between proximal and distal regions was visually inspected using multiphoton microscope (Fig. 6). Collagen appears to be highly dense, corrugated, and hard to trace in proximal regions. Whereas in distal regions it seems to be less undulated with a more defined and traceable structure. This was further confirmed by the quantification of waviness for SHG images of adventitial collagen (Fig. 7).

These results are in line with other observations; Martin et al. [24] reported a stiffer material property for the human aorta compared to the porcine aorta and associated the stiffer property with less elastin content as well as collagen waviness in the human tissue. Using inflation tests, Lillie et al. [25] described that the circumferential stretch at which the first collagen recruitment takes place, decreases along the thoracic aorta. Collagen waviness in the thoracic aorta was found to be inversely correlated with age [50,68]. Recently, we showed that gradual digestion of elastin from load-free aortic tissues clearly reduces the collagen waviness [27,49], in agreement with other reports [69,70]. Although we have not quantified elastin content nor included the mass (volume) fractions in constitutive models, these studies together with our observation suggest that there is a coupling between elastin and collagen and possibly a relationship between content and structure of wall constituents.

Variations Through Multiple Layers of Aorta. For each layer of media and adventitia, we assumed the same constitutive form but independent material parameters [30,40]. Model predictions for the recruitment distributions suggest that the medial collagen engages in load bearing from the onset of loading whereas the adventitial collagen is being recruited at a later stage of stretching (Fig. 3). Indeed, our recent multiphoton image analysis of biaxially stretched aortic tissues showed that medial collagen appears to be engaged throughout the stretching process while the adventitial collagen is engaged only after 20% of equibiaxial strain [27]. A transmural difference in the recruitment threshold of collagen fibers was also indicated using two-photon microscopy for carotid arteries [66]. Together, these findings demonstrate differential engagement of collagen fibers between aortic layers and imply the importance of constitutive formulations with layer-specific structural properties. This differential engagement of collagen add more emphasis on the well-known role of adventitial collagen in preventing the aorta from over inflation [1].

A significantly larger ratio of elastin material constants between media and adventitia was predicted ($c_e^M/c_e^A > 20$), which is slightly above the range ($6 < c_e^M/c_e^A < 14$) previously suggested by Holzapfel et al. [30]. Indeed, multiphoton microscopy in the current as well as our previous studies did not capture any signal from elastin in the adventitia, at least within 60 μm depth from the outermost layer of the adventitia [27,49]. These results together with the observation of higher Young's modulus for the media compared to the adventitia under low stretches [71], lend more support to the notion that elastin constitutes only a small portion of the adventitia compared to the media [15].

The intrinsic elastic property of collagen in each layer (c_c^M, c_c^A) was considered to be independent of the axial location along the aorta. Indeed, this parameter showed only a minor change from thoracic to abdominal regions [68] with a weak correlation with age [50] using similar recruitment-based models. We chose to fix these values based on the suggested values in the literature in order to solely look for the possible structural variations of collagen and also to reduce the number of optimization parameters and, hence, the nonunique solutions.

Collagen fiber families in the media and adventitia were found to be mainly oriented toward circumferential and longitudinal directions, respectively (Tables 2 and 3), consistent with other studies [27,30,35,72,]. In addition, Schriefl et al. [35] reported no

Table 3 Parameters of model C estimated for aortic samples at four locations (proximal, midproximal, mid-distal, and distal) along three thoracic aortas

	c_e^M (kPa)	c_e^A (kPa)	α^M	β^M	α^A	β^A	γ^M	γ^A	RMS
Proximal									
Artery1	121.06	2.64	1.72	1.75	2.66	1.62	33.50	67.80	47.52
Artery2	124.22	5.00	1.30	4.63	3.75	0.33	31.56	55.80	28.62
Artery3	130.31	0.12	1.41	2.62	2.70	0.82	30.69	60.90	22.64
Artery4	102.57	4.85	1.22	5.10	4.08	0.36	28.42	60.99	33.80
Artery5	182.91	4.26	1.23	4.84	3.47	0.40	25.96	50.78	57.89
Mean	132.21	3.37	1.38	3.79	3.33	0.71	30.03	59.25	
Midproximal									
Artery1	139.88	4.79	1.87	1.36	3.45	0.70	34.69	67.34	50.31
Artery2	117.93	1.19	0.74	62.16	2.62	0.68	27.48	50.93	28.70
Artery3	116.80	3.20	1.22	3.57	2.34	1.96	32.30	61.23	42.24
Artery4	128.23	3.34	1.30	5.69	3.87	0.40	34.13	62.00	38.85
Artery5	222.51	3.80	1.26	4.48	2.77	0.47	28.01	52.56	44.14
Mean	145.07	3.26	1.28	15.45	3.01	0.84	31.32	58.81	
Mid-distal									
Artery1	236.33	0.19	1.76	0.88	3.20	0.51	30.56	66.00	89.28
Artery2	154.21	0.23	1.61	1.23	3.10	0.44	29.19	50.70	46.59
Artery3	202.65	0.20	1.74	0.78	2.11	0.71	30.46	59.30	54.88
Artery4	115.50	3.87	1.07	5.73	3.47	0.43	36.62	60.85	70.26
Artery5	201.41	3.24	1.03	8.05	3.75	0.34	33.56	53.68	53.55
Mean	182.02	1.55	1.44	3.33	3.13	0.49	32.08	58.11	
Distal									
Artery1	153.87	0.71	2.40	0.43	4.07	0.20	20.17	53.76	93.58
Artery2	189.80	1.18	2.45	0.30	5.25	0.12	31.52	51.81	54.75
Artery3	220.44	2.21	1.60	0.93	3.81	0.17	24.71	47.55	63.42
Artery4	103.54	3.91	1.12	6.45	3.42	0.44	33.27	52.24	74.03
Artery5	138.88	4.99	1.01	6.32	3.27	0.46	31.55	57.71	128.73
Mean	161.31	2.60	1.72	2.89	3.96	0.28	28.24	52.61	

significant variation in preferred collagen fiber directions along the aorta from thoracic to abdominal regions, in parallel with our model predictions (Tables 2 and 3).

Note that in this study an integrated contribution of elastin and collagen of multiple arterial layers to the total behavior of the aortic wall was modeled, disregarding the possible structural and mechanical coupling between multiple layers. A number of studies has investigated the layer specific mechanical properties through dissection and testing of individual arterial layers [36,38,73]. The layered inhomogeneity of soft tissue properties has also been investigated with other techniques such as pipette aspiration [74].

Model Comparison and Parameter Sensitivity Analysis. Each model in this study introduced eight unknown parameters to the nonlinear least squares problem while showing minimal differences in the goodness-of-fit (Tables 1–3). Models B and C assumed linear behavior for individual fibers when engaged but considered the Normal and Gamma statistical distributions for the engagement. Other forms of statistical distributions have been suggested and used in literature as well [43,65]. In our study, both models were able to characterize the differences in fiber engagement dynamics between layers while describing the variation of properties along the aorta. In model A, the intrinsic properties of collagen fibers and their gradual engagement in load bearing were represented with an exponential function. While model A also showed an increasing contribution of collagen fibers along the length of aorta, it is difficult to interpret the sequence of fiber engagement between the two layers using this model.

Parameter sensitivity analysis is a study used in many fields as a tool to assess the identifiability of model parameters and the design of experiments using nonlinear regression [58]. Valentín and Humphrey [75] studied the sensitivity of a mixture model of arterial growth and remodeling to the changes in parameters associated with the matrix turnover. Ellwein et al. [57] analyzed the sensitivity of the lumped parameter models predicting blood flow and pressure in cardiovascular systems. The analysis of sensitivity in this study showed that the recruitment-based models are more sensitive to variations in the respective constitutive parameters compared to the exponential-based model (Fig. 5). However, the linear dependency of sensitivity coefficients observed for the recruitment-based models may cause difficulties in terms of the convergence and even the nonunique solutions (see Ref. [58] for a detailed discussion).

Limitations

One of the main challenges of nonlinear least squares problems with large number of unknown variables is the existence of multiple local minima [58,76,77]. To address this issue, the optimization was repeated with several initial points to assure the optimality of the solutions. Porcine thoracic aorta is a relatively thick artery and the difference in waviness between proximal and distal locations using multiphoton microscopy was observed only over 100 μm thickness. Also, advanced quantitative analysis of fiber engagement under mechanical loading and its variation with location are ultimately needed. Our ongoing studies suggest that there are no significant changes in the opening angle along the thoracic aorta. Such results are consistent with the earlier report by Han and Fung [78]. Therefore, we do not expect much correlation between collagen undulation and residual stress quantified through the opening angle tests. The in vivo axial stretch, however, may be correlated with the overall collagen undulation which deserves to be investigated more thoroughly. Inclusion of mass (volume) fraction of constituents [43] corresponding to different regions of interest along the aorta could improve the model predictions. Constitutive models with distributed collagen fiber orientation would provide a better match with the image analysis of fiber dispersion compared to models with multiple families of parallel fibers [34,45,47,64,79–81]. Also extending the constitutive models to include the passive contribution of smooth muscle

cell [82–85] would complement our models although its contribution to the passive stiffness of the wall is known to be much less than the extracellular matrix [3].

Conclusions

The degree of collagen undulation was demonstrated to be a factor leading to the difference in mechanical properties along the thoracic aorta. Bilayer recruitment-based constitutive models were able to capture a sequence for collagen recruitment between arterial layers. That is, medial collagen recruitment occurs early from the beginning of loading followed by the recruitment of adventitial collagen. Current study underscores the need for further studies on the constitutive models that account for the layer-specific collagen engagement dynamics with the help of advanced microscopic imaging.

Acknowledgment

This work has been supported by the National Heart, Lung, and Blood Institute Grant No. R01 HL-098028. The authors would like to thank Professor Charles P. Lin from the Center for Systems Biology and Wellman Center for Photomedicine, Harvard Medical School, for providing access to the multiphoton microscope.

Appendix

A Convexity Study of the Constitutive Models

For details of the convexity of model A see, Holzapfel et al. [30] and Gasser et al. [34]. Herein let's focus on model B and, for simplicity, consider the artery as one layer of collagenous tissue with symmetric fiber families. Then, the strain energy function (Eq. (2)) is rewritten as

$$W(\lambda_z, \lambda_\theta) = \psi(E) = \int_0^E \psi_f(E - x)\rho_f(x)dx \tag{A1}$$

where $\psi_f = 1/2c_cE^2$, $E = 1/2(\lambda_z^2 \sin^2\gamma + \lambda_\theta^2 \cos^2\gamma - 1)$, and γ is the absolute value of the fiber family orientations with respect to the circumference. Assuming $c_c > 0$, it is easy to show that $\psi(E) > 0, \psi'(E) > 0, \psi''(E) > 0$ and also

$$W_p = \psi' E_p, W_{pq} = \psi'' E_p E_q + \psi' E_{pq} \tag{A2}$$

where subscripts p and q indicate the partial derivatives with respect to principal stretches λ_z or λ_θ, i.e., $p, q \in \{z, \theta\}$. It can be shown $W_{zz} > 0$ and, therefore, $W(\lambda_z, \lambda_\theta)$ is considered to be strictly convex if the determinant of the Hessian matrix is positive as [34]

$$W_{zz}W_{\theta\theta} - W_{z\theta}^2 = \psi''\psi' E_\theta^2 E_{\theta\theta} + \psi''\psi' E_z^2 E_{\theta\theta} + \psi'^2 E_{zz}E_{\theta\theta} > 0 \tag{A3}$$

In the same fashion, the convexity of the model with two layers can be shown.

References

[1] Humphrey, J. D., 2002, *Cardiovascular Solid Mechanics: Cells, Tissues, and Organs*, Springer, New York.
[2] Kassab, G. S., 2006, "Biomechanics of the Cardiovascular System: The Aorta as an Illustratory Example," J. R. Soc. Interface, **3**(11), pp. 719–740.
[3] Burton, A. C., 1954, "Relation of Structure to Function of the Tissues of the Wall of Blood Vessels," Physiol. Rev., **34**(4), pp. 619–642.
[4] Wolinsky, H., and Glagov, S., 1964, "Structural Basis for the Static Mechanical Properties of the Aortic Media," Circ. Res., **14**(5), pp. 400–413.
[5] Roach, M. R., and Burton, A. C., 1957, "The Reason for the Shape of the Distensibility Curves of Arteries," Can. J. Biochem. Physiol., **35**(8), pp. 681–690.
[6] Fung, Y. C., Fronek, K., and Patitucci, P., 1979, "Pseudoelasticity of Arteries and the Choice of Its Mathematical Expression," Am. Physiol. Soc., **237**(5), pp. H620–H631.
[7] Tsamis, A., Krawiec, J. T., and Vorp, D. A., 2013, "Elastin and Collagen Fibre Microstructure of the Human Aorta in Ageing and Disease: A Review," J. R. Soc. Interface, **10**(83), p. 20121004.
[8] García-Herrera, C. M., Celentano, D. J., Cruchaga, M. A., Rojo, F. J., Atienza, J. M., Guinea, G. V., and Goicolea, J. M., 2012, "Mechanical Characterisation of the Human Thoracic Descending Aorta: Experiments and Modelling," Comput. Methods Biomech. Biomed. Eng., **15**(2), pp. 185–193.
[9] Zou, Y., and Zhang, Y., 2009, "An Experimental and Theoretical Study on the Anisotropy of Elastin Network," Ann. Biomed. Eng., **37**(8), pp. 1572–1583.
[10] Rouleau, L., Tremblay, D., Cartier, R., Mongrain, R., and Leask, R. L., 2012, "Regional Variations in Canine Descending Aortic Tissue Mechanical Properties Change With Formalin Fixation," Cardiovasc. Pathol., **21**(5), pp. 390–397.
[11] Kim, J., Hong, J. W., and Baek, S., 2013, "Longitudinal Differences in the Mechanical Properties of the Thoracic Aorta Depend on Circumferential Regions," J. Biomed. Mater. Res. A., **101**(5), pp. 1525–1529.
[12] Labrosse, M. R., Beller, C. J., Mesana, T., and Veinot, J. P., 2009, "Mechanical Behavior of Human Aortas: Experiments, Material Constants and 3D Finite Element Modeling Including Residual Stress," ASME J. Biomech. Eng., **42**(8), pp. 996–1004.
[13] Roccabianca, S., Figueroa, C. A., Tellides, G., and Humphrey, J. D., 2014, "Quantification of Regional Differences in Aortic Stiffness in the Aging Human," J. Mech. Behav. Biomed. Mater., **29**, pp. 618–634.
[14] Harkness, M. L., Harkness, R. D., and McDonald, D. A., 1957, "The Collagen and Elastin Content of the Arterial Wall in the Dog," Proc. R. Soc. London, Ser. B, **146**(925), pp. 541–551.
[15] Sokolis, D. P., 2007, "Passive Mechanical Properties and Structure of the Aorta: Segmental Analysis," Acta Physiol., **190**(4), pp. 277–289.
[16] Halloran, B. G., Davis, V. A., McManus, B. M., Lynch, T. G., and Baxter, B. T., 1995, "Localization of Aortic Disease Is Associated With Intrinsic Differences in Aortic Structure," J. Surg. Res., **59**(1), pp. 17–22.
[17] Cheuk, B. L., and Cheng, S. W., 2005, "Expression of Integrin Alpha5beta1 and the Relationship to Collagen and Elastin Content in Human Suprarenal and Infrarenal Aortas," Vasc. Endovasc. Surg., **39**(3), pp. 245–251.
[18] Wolinsky, H., and Glagov, S., 1969, "Comparison of Abdominal and Thoracic Aortic Medial Structure in Mammals," Circ. Res., **25**(6), pp. 677–686.
[19] Sokolis, D. P., Boudoulas, H., Kavantzas, N. G., Kostomitsopoulos, N., Agapitos, E. V., and Karayannacos, P. E., 2002, "A Morphometric Study of the Structural Characteristics of the Aorta in Pigs Using an Image Analysis Method," Anat., Histol., Embryol., **31**(1), pp. 21–30.
[20] Purslow, P. P., 1983, "Positional Variations in Fracture Toughness, Stiffness and Strength of Descending Thoracic Pig Aorta," ASME J. Biomech. Eng., **16**(11), pp. 947–953.
[21] Guo, X., and Kassab, G. S., 2003, "Variation of Mechanical Properties Along the Length of the Aorta in C57bl/6 Mice," Am. J. Physiol. Heart Circ. Physiol., **285**(6), pp. H2614–H2622.
[22] Haskett, D., Johnson, G., Zhou, A., Utzinger, U., and Vande Geest, J., 2010, "Microstructural and Biomechanical Alterations of the Human Aorta as a Function of Age and Location," Biomech. Model Mechanobiol., **9**(6), pp. 725–736.
[23] Rachev, A., Greenwald, S., and Shazly, T., 2013, "Are Geometrical and Structural Variations Along the Length of the Aorta Governed by a Principle of "Optimal Mechanical Operation?," ASME J. Biomech. Eng., **135**(8), p. 081006.
[24] Martin, C., Pham, T., and Sun, W., 2011, "Significant Differences in the Material Properties Between Aged Human and Porcine Aortic Tissues," Eur. J. Cardiothorac. Surg., **40**(1), pp. 28–34.
[25] Lillie, M. A., Armstrong, T. E., Gérard, S. G., Shadwick, R. E., and Gosline, J. M., 2012, "Contribution of Elastin and Collagen to the Inflation Response of the Pig Thoracic Aorta: Assessing Elastin's Role in Mechanical Homeostasis," ASME J. Biomech. Eng., **45**(12), pp. 2133–2141.
[26] Lindeman, J. H. N., Ashcroft, B. A., Beenakker, J. W. M., Es, M. V., Koekkoek, N. B. R., Prins, F. A., Tielemans, J. F., Abdul-Hussien, H., Bank, R. A., and Oosterkamp, T. H., 2010, "Distinct Defects in Collagen Microarchitecture Underlie Vessel-Wall Failure in Advanced Abdominal Aneurysms and Aneurysms in Marfan Syndrome," Proc. Natl. Acad. Sci. U. S. A., **107**(2), pp. 862–865.
[27] Chow, M. J., Turcotte, R., Lin, C. P., and Zhang, Y., 2014, "Arterial Extracellular Matrix: A Mechanobiological Study of the Contributions and Interactions of Elastin and Collagen," Biophys. J., **106**(12), pp. 2684–2692.
[28] Chow, M. J., Mondonedo, J. R., Johnson, V. M., and Zhang, Y., 2013, "Progressive Structural and Biomechanical Changes in Elastin Degraded Aorta," Biomech. Model. Mechanobiol., **12**(2), pp. 361–372.
[29] Sacks, M. S., 1999, "A Method for Planar Biaxial Mechanical Testing That Includes In-Plane Shear," ASME J. Biomech. Eng., **121**(5), pp. 551–555.
[30] Holzapfel, G. A., Gasser, T. C., and Ogden, R. W., 2000, "A New Constitutive Framework for Arterial Wall Mechanics and a Comparative Study of Material Models," J. Elasticity, **61**(3), pp. 1–48.
[31] Humphrey, J. D., 2003, "Continuum Biomechanics of Soft Biological Tissues," Proc. R. Soc. London, Ser. A, **459**(2029), pp. 3–46.
[32] Holzapfel, G. A., and Ogden, R. W., 2010, "Constitutive Modelling of Arteries," Proc. R. Soc. London, Ser. A, **466**(2118), pp. 1551–1597.
[33] Alastrué, V., Sáez, P., Martínez, M. A., and Doblaré, M., 2010, "On the Use of the Bingham Statistical Distribution in Microsphere-Based Constitutive Models for Arterial Tissue," Mech. Res. Commun., **37**(8), pp. 700–706.

[34] Gasser, T. C., Ogden, R. W., and Holzapfel, G. A., 2006, "Hyperelastic Modelling of Arterial Layers With Distributed Collagen Fibre Orientations," J. R. Soc. Interface, **3**(6), pp. 15–35.
[35] Schriefl, A. J., Zeindlinger, G., Pierce, D. M., Regitnig, P., and Holzapfel, G. A., 2012, "Determination of the Layer-Specific Distributed Collagen Fibre Orientations in Human Thoracic and Abdominal Aortas and Common Iliac Arteries," J. R. Soc. Interface, **9**(71), pp. 1275–1286.
[36] Sommer, G., Regitnig, P., Költringer, L., and Holzapfel, G. A., 2010, "Biaxial Mechanical Properties of Intact and Layer-Dissected Human Carotid Arteries at Physiological and Supraphysiological Loadings," Am. J. Physiol. Heart Circ. Physiol., **298**(3), pp. H898–H912.
[37] von Maltzahn, W. W., Besdo, D., and Wiemer, W., 1981, "Elastic Properties of Arteries: A Nonlinear Two-Layer Cylindrical Model," ASME J. Biomech. Eng., **14**(6), pp. 389–397.
[38] Sokolis, D. P., Kritharis, E. P., and Iliopoulos, D. C., 2012, "Effect of Layer Heterogeneity on the Biomechanical Properties of Ascending Thoracic Aortic Aneurysms," Med. Biol. Eng. Comput., **50**(12), pp. 1227–1237.
[39] Holzapfel, G. A., 2000, *Nonlinear Solid Mechanics: A Continuum Approach for Engineering*, Wiley, New York.
[40] Badel, P., Avril, S., Lessner, S., and Sutton, M., 2012, "Mechanical Identification of Layer-Specific Properties of Mouse Carotid Arteries Using 3D-DIC and a Hyperelastic Anisotropic Constitutive Model," Comput. Methods Biomech. Biomed. Eng., **15**(1), pp. 37–48.
[41] Lanir, Y., 1979, "A Structural Theory for the Homogeneous Biaxial Stress–Strain Relationships in Flat Collagenous Tissues," ASME J. Biomech. Eng., **12**(6), pp. 423–436.
[42] Wuyts, F. L., Vanhuyse, V. J., Langewouters, G. J., Decraemer, W. F., Raman, E. R., and Buyle, S., 1995, "Elastic Properties of Human Aortas in Relation to Age and Atherosclerosis: A Structural Model," Phys. Med. Biol., **40**(10), pp. 1577–1597.
[43] Zulliger, M. A., Frideza, P., Hayashi, K., and Stergiopulos, N., 2004, "A Strain Energy Function for Arteries Accounting for Wall Composition and Structure," ASME J. Biomech. Eng., **37**(7), pp. 989–1000.
[44] Cacho, F., Elbischger, P. J., Rodríguez, J. F., Doblaré, M., and Holzapfel, G. A., 2007, "A Constitutive Model for Fibrous Tissues Considering Collagen Fiber Crimp," Int. J. Nonlinear Mech., **42**, pp. 391–402.
[45] Sacks, M. S., 2003, "Incorporation of Experimentally-Derived Fiber Orientation Into a Structural Constitutive Model for Planar Collagenous Tissues," ASME J. Biomech. Eng., **125**(2), pp. 280–287.
[46] Sacks, M. S., and Sun, W., 2003, "Multiaxial Mechanical Behavior of Biological Materials," Annu. Rev. Biomed. Eng., **5**(1), pp. 251–284.
[47] Hill, M. R., Duan, X., Gibson, G. A., Watkins, S., and Robertson, A. M., 2012, "A Theoretical and Non-Destructive Experimental Approach for Direct Inclusion of Measured Collagen Orientation and Recruitment Into Mechanical Models of the Artery Wall," ASME J. Biomech. Eng., **45**(5), pp. 762–771.
[48] Rezakhaniha, R., Fonck, E., Genoud, C., and Stergiopulos, N., 2011, "Role of Elastin Anisotropy in Structural Strain Energy Functions of Arterial Tissue," Biomech. Model. Mechanobiol., **10**(4), pp. 599–611.
[49] Zeinali-Davarani, S., Chow, M. J., Turcotte, R., and Zhang, Y., 2013, "Characterization of Biaxial Mechanical Behavior of Porcine Aorta Under Gradual Elastin Degradation," Ann. Biomed. Eng., **41**(7), pp. 1528–1538.
[50] Zulliger, M. A., and Stergiopulos, N., 2007, "Structural Strain Energy Function Applied to the Ageing of the Human Aorta," ASME J. Biomech. Eng., **40**(14), pp. 3061–3069.
[51] Agianniotis, A., Rezakhaniha, R., and Stergiopulos, N., 2011, "A Structural Constitutive Model Considering Angular Dispersion and Waviness of Collagen Fibres of Rabbit Facial Veins," Biomed. Eng., **10**, p. 18.
[52] Buck, R. C., 1987, "Collagen Fibril Diameter in the Common Carotid Artery of the Rat," Connect. Tissue Res., **16**(2), pp. 121–129.
[53] Merrilees, M. J., Tiang, K. M., and Scott, L., 1987, "Changes in Collagen Fibril Diameters Across Artery Walls Including a Correlation With Glycosaminoglycan Content," Connect. Tissue Res., **16**(3), pp. 237–257.
[54] Dingemans, K. P., Teeling, P., Lagendijk, J. H., and Becker, A. E., 2000, "Extracellular Matrix of the Human Aortic Media: An Ultrastructural Histochemical and Immunohistochemical Study of the Adult Aortic Media," Anat. Rec., **258**(1), pp. 1–14.
[55] Eriksen, H. A., Pajala, A., Leppilahti, J., and Risteli, J., 2002, "Increased Content of Type III Collagen at the Rupture Site of Human Achilles Tendon," J. Orthop. Res., **20**(6), pp. 1352–1357.
[56] Wagner, H. P., and Humphrey, J. D., 2011, "Differential Passive and Active Biaxial Mechanical Behaviors of Muscular and Elastic Arteries: Basilar Versus Common Carotid," ASME J. Biomech. Eng., **133**(5), p. 051009.
[57] Ellwein, L. M., Tran, H. T., Zapata, C., Novak, V., and Olufsen, M. S., 2008, "Sensitivity Analysis and Model Assessment: Mathematical Models for Arterial Blood Flow and Blood Pressure," Cardiovasc. Eng., **8**(2), pp. 94–108.
[58] Beck, J. V., and Arnold, K. J., 1977, *Parameter Estimation in Engineering and Science*, Wiley, New York.
[59] Zoumi, A., Lu, X., Kassab, G. S., and Tromberg, B. J., 2004, "Imaging Coronary Artery Microstructure Using Second-Harmonic and Two-Photon Fluorescence Microscopy," Biophys. J., **87**(4), pp. 2778–2786.
[60] Veilleux, I., Spencer, J. A., Biss, D. P., and Lin, C. P., 2008, "In Vivo Cell Tracking With Video Rate Multimodality Laser Scanning Microscopy," IEEE J. Sel. Top. Quantum Electron., **14**(1), pp. 10–18.
[61] Meijering, E., Jacob, M., Sarria, J. C., Steiner, P., Hirling, H., and Unser, M., 2004, "Design and Validation of a Tool for Neurite Tracing and Analysis in Fluorescence Microscopy Images," Cytometry, Part A, **58**(2), pp. 167–176.
[62] Meijering, E., 2010, "Neuron Tracing in Perspective," Cytometry, Part A, **77**(7), pp. 693–704.
[63] Schriefl, A. J., Collins, M. J., Pierce, D. M., Holzapfel, G. A., Niklason, L. E., and Humphrey, J. D., 2012, "Remodeling of Intramural Thrombus and Collagen in an Ang-II Infusion ApoE/Model of Dissecting Aortic Aneurysms," Thromb. Res., **130**(3), pp. e139–e146.
[64] Fata, B., Carruthers, C. A., Gibson, G., Watkins, S. C., Gottlieb, D., Mayer, J. E., and Sacks, M. S., 2013, "Regional Structural and Biomechanical Alterations of the Ovine Main Pulmonary Artery During Postnatal Growth," ASME J. Biomech. Eng., **135**(3–4), p. 021022.
[65] Rezakhaniha, R., Agianniotis, A., Schrauwen, J. T. C., Griffa, A., Sage, D., Bouten, C. V. C., van de Vosse, F. N., Unser, M., and Stergiopulos, N., 2012, "Experimental Investigation of Collagen Waviness and Orientation in the Arterial Adventitia Using Confocal Laser Scanning Microscopy," Biomech. Model. Mechanobiol., **11**(3–4), pp. 461–473.
[66] Wang, R., Brewster, L. P., and Gleason, R. L., 2013, "In-Situ Characterization of the Uncrimping Process of Arterial Collagen Fibers Using Two-Photon Confocal Microscopy and Digital Image Correlation," ASME J. Biomech. Eng., **46**(15), pp. 2726–2729.
[67] Tanaka, T. T., and Fung, Y. C., 1974, "Elastic and Inelastic Properties of the Canine Aorta and Their Variation Along the Aortic Tree," ASME J. Biomech. Eng., **7**(4), pp. 357–370.
[68] Fonck, E., Prod'hom, G., Roy, S., Augsburger, L., Rufenacht, D. A., and Stergiopulos, N., 2007, "Effect of Elastin Degradation on Carotid Wall Mechanics as Assessed by a Constituent-Based Biomechanical Model," Am. J. Physiol. Heart. Circ. Physiol., **292**(6), pp. H2754–H2763.
[69] Ferruzzi, J., Collins, M. J., Yeh, A. T., and Humphrey, J. D., 2011, "Mechanical Assessment of Elastin Integrity in Fibrillin-1-Deficient Carotid Arteries: Implications for Marfan Syndrome," Cardiovasc. Res., **92**(2), pp. 287–295.
[70] Yu, Q., Zhou, J., and Fung, Y. C., 1993, "Neutral Axis Location in Bending and Young's Modulus of Different Layers of Arterial Wall," Am. J. Physiol., **265**(1), pp. H52–H60.
[71] O'Connell, M. K., Murthy, S., Phan, S., Xu, C., Buchanan, J., Spilker, R., Dalman, R., L., Zarins, C. K., Denk, W., and Taylor, C. A., 2008, "The Three-Dimensional Micro- and Nanostructure of the Aortic Medial Lamellar Unit Measured Using 3D Confocal and Electron Microscopy Imaging," Matrix Biol., **27**(3), pp. 171–181.
[72] Holzapfel, G. A., Sommer, G., Gasser, T. C., and Regitnig, P., 2005, "Determination of Layer-Specific Mechanical Properties of Human Coronary Arteries With Nonatherosclerotic Intimal Thickening and Related Constitutive Modeling," Am. J. Physiol. Heart Circ. Physiol., **289**(5), pp. H2048–H2058.
[73] Aoki, T., Ohashi, T., Matsumoto, T., and Sato, M., 1997, "The Pipette Aspiration Applied to the Local Stiffness Measurement of Soft Tissues," Ann. Biomed. Eng., **25**(3), pp. 581–587.
[74] Valentín, A., and Humphrey, J. D., 2009, "Parameter Sensitivity Study of a Constrained Mixture Model of Arterial Growth and Remodeling," ASME J. Biomech. Eng., **131**(10), p. 101006.
[75] Ogden, R. W., Saccomandi, G., and Sgura, I., 2004, "Fitting Hyperelastic Models to Experimental Data," Comput. Mech., **34**(6), pp. 484–502.
[76] Zeinali-Davarani, S., Choi, J., and Baek, S., 2009, "On Parameter Estimation for Biaxial Mechanical Behavior of Arteries," ASME J. Biomech. Eng., **42**(4), pp. 524–530.
[77] Han, H. C., and Fung, Y. C., 1991, "Species Dependence of the Zero-Stress State of Aorta: Pig Versus Rat," ASME J. Biomech. Eng., **113**(4), pp. 446–451.
[78] Wan, W., Dixon, J. B., and Gleason, R. L. Jr., 2012, "Constitutive Modeling of Mouse Carotid Arteries Using Experimentally Measured Microstructural Parameters," Biophys. J., **102**(12), pp. 2916–2925.
[79] Gasser, T. C., Gallinetti, S., Xing, X., Forsell, C., Swedenborg, J., and Roy, J., 2012, "Spatial Orientation of Collagen Fibers in the Abdominal Aortic Aneurysm's Wall and Its Relation to Wall Mechanics," Acta Biomater., **8**(8), pp. 3091–3103.
[80] Lokshin, O., and Lanir, Y., 2009, "Micro and Macro Rheology of Planar Tissues," Biomaterials, **30**(17), pp. 3118–3127.
[81] Gleason, R. L., Taber, L. A., and Humphrey, J. D., 2004, "A 2D Model of Flow-Induced Alterations in the Geometry, Structure, and Properties of Carotid Arteries," ASME J. Biomech. Eng., **126**(3), pp. 371–381.
[82] Valentín, A., Cardamone, L., Baek, S., and Humphrey, J. D., 2009, "Complementary Vasoactivity and Matrix Remodelling in Arterial Adaptations to Altered Flow and Pressure," J. R. Soc. Interface, **6**(32), pp. 293–306.
[83] Hansen, L., Wan, W., and Gleason, R. L., 2009, "Microstructurally Motivated Constitutive Modeling of Mouse Arteries Cultured Under Altered Axial Stretch," ASME J. Biomech. Eng., **131**(10), p. 101015.
[84] Bellini, C., Ferruzzi, J., Roccabianca, S., Di Martino, E. S., and Humphrey, J. D., 2014, "A Microstructurally Motivated Model of Arterial Wall Mechanics With Mechanobiological Implications," Ann. Biomed. Eng., **42**(3), pp. 488–502.
[85] Zeinali-Davarani, S., Raguin, L. G., Vorp, D. A., and Baek, S., 2011, "Identification of In Vivo Material and Geometric Parameters of a Human Aorta: Toward Patient Specific Modeling of Abdominal Aortic Aneurysm," Biomech. Model Mechanobiol., **10**(5), pp. 689–699.